PHYSICAL REVIEW B **82**, 144117 (2010)

First-principles thermodynamic modeling of atomic ordering in yttria-stabilized zirconia

P. Dalach,[1] D. E. Ellis,[1,*] and A. van de Walle[2]
[1]*Department of Physics and Astronomy, Northwestern University, Evanston, Illinois 60208, USA*
[2]*Department of Engineering and Applied Science Division, California Institute of Technology, Pasadena, California 91125, USA*

(Received 23 July 2010; revised manuscript received 5 October 2010; published 26 October 2010)

Yttria-stabilized zirconia (YSZ) is modeled using a cluster expansion statistical thermodynamics method built upon a density-functional theory database. The reliability of cluster expansions in predicting atomic ordering is explored by comparing with the extensive experimental database. The cluster expansion of YSZ is utilized in lattice Monte Carlo simulations to compute the ordering of dopant and oxygen vacancies as a function of concentration. Cation dopants show a strong tendency to aggregate and vacate significantly sized domains below 9 mol % Y_2O_3, which is likely important for YSZ aging processes in ionic conductivity. Evolution of vibrational and underlying electronic properties as a function of Y doping is explored.

DOI: 10.1103/PhysRevB.82.144117 PACS number(s): 61.72.Bb, 66.30.Dn

I. INTRODUCTION

There has been increased interest in solid oxide fuel cells (SOFCs) in recent years as a means to efficiently generate clean electricity from domestic fuel sources. For this reason, SOFC material components have come under increased scrutiny as a means to reach government benchmarks that would allow fuel cells to become economically competitive with other means of commercially available power production.[1] The search for materials to optimize SOFC performance has largely been carried out in the traditional trial and error basis, by extension of existing databases and by extrapolating material properties. Systematic and rapid improvements of fuel cell component materials will require both an atomistic and statistical understanding of the structure and defects of proposed materials but few tools exist to give a rational design basis for systematic improvements. It is therefore necessary to develop tools that can help researchers correlate atom-level ordering to dynamic material properties, using that knowledge to build better functioning materials.

Yttria-stabilized zirconia (YSZ), Y_2O_3 doped into ZrO_2, is the prototypical SOFC material. YSZ is extensively used for both the electrolyte and as a part of both electrode components due to its high oxygen diffusivity at elevated temperatures and poor electronic conductivity. A vast body of literature exists on YSZ, including studies on atomic ordering of particular interest here[2–4] (for experimental and theoretical background, see Refs. 3 and 4 and references therein). Additional theoretical first-principles work which helps characterize the ionic conductivity of YSZ as a function of direct atom-atom and atom-defect interactions is of interest. It has been suggested that extended aggregations of vacancies larger than can be realistically simulated using molecular dynamics[3] may give insight into experimental diffusion and conductivity results.[5] Methods that can include extended atomic features >1 nm are necessary.

Cluster expansion (CE) methods, enabling first-principles-based thermodynamic models, are introduced to obtain atomic ordering data. Previously, CE methods have been successfully used in calculating alloy phase diagrams,[6] predicting new material ground states,[7] exploring diffusion mechanisms in Li intercalated systems,[8,9] and discerning the composition of ceria interfaces.[10] In this work, CE methods are applied to YSZ to gain distinct insight into dopant/vacancy ordering properties.

YSZ was chosen for two reasons. (1) There are still outstanding questions concerning the dependence of oxygen ion conduction on both yttrium content and the high-temperature aging of the material. Specifically, though increasing yttrium content boosts the mobile charge carriers (oxygen vacancies), ionic conduction decreases above 8 mol % Y_2O_3. Additionally, though materials above 9 mol % Y_2O_3 show minimal ionic conduction losses with aging at typical SOFC operating temperatures (usually >1000 K), materials below this level of yttrium experience radical decreases in ionic conductivity.[11] (2) The quality of the atomic ordering results derived from CE methods can be evaluated by comparison with the extensive YSZ literature on atomic ordering. As this work was completed, unpublished work on YSZ that considers related questions using similar methodology was discovered.[12,13] These earlier studies did not include infinite-range electrostatic interactions, the effect of lattice vibrations or a formal-charge-dependent cluster expansion. Finally, this work was done as preparation for applications to next generation perovskite-structure SOFC component materials where experimental data are not as plentiful.

II. METHODOLOGY

A. Energy cluster expansion

Cluster expansion methods fit libraries of structures with known material properties, such as bulk and surface energy, elasticity, piezoelectricity, dielectric constants, optoelectric coupling, and anisotropic diffusion coefficients,[14] to a summation over small clusters of atomic sites consisting mostly of short-range pair and triplet interactions.[15] CE methods produce semianalytical equations for the desired property using concentration and configuration space of a single topological structure as component variables. First-principles methods such as density-functional theory (DFT) (widely used to determine equilibrated atomic positions, energies, magnetic ordering, etc.) have a practical size limit of approximately 200 atoms/cell due to computational cost. CE methods, however, can marry first-principles approaches to statistical algorithms such as Monte Carlo, allowing simulations at finite temperature of realistically sized, nanostructured systems. CE methods can be extended to include vacancy and interstitial defects, which are of obvious importance in studying atomic ordering in ionic conductors. As CE expansion parameters are "trained" using material properties determined via first principles, this method presents an attractive compromise between the rigorous but time-consuming first-principles level of theory and faster, more generalized statistical methods.

The thermodynamic approach used is embodied in the Alloy Theoretic Automated Toolkit[16] (ATAT) employed to generate a lattice energy CE for target materials,

$$E(\sigma) = \sum_{\alpha} m_{\alpha} J_{\alpha} \langle \varphi_{\alpha}(\vec{\sigma}) \rangle. \tag{1}$$

Here m_α is the multiplicity of cluster α, J_α are the variational coefficients of cluster α, and $\langle \varphi_\alpha(\sigma) \rangle$ is the lattice average of the cluster functions defining distinct site groupings. The cluster coefficients, J_α, contain the structural energy information from systems in the training library. As the clusters are initially fit to DFT derived energies, these coefficients represent zero temperature (T) $T=0$ K structural energy information. The coefficients are found by fitting clusters, usually including short-range pairs, triplets, quadruplets, etc., to a relatively small number of $N \sim 10^2$ energies obtained from first-principles calculations. It must be noted that though these clusters are tied to a single underlying topological lattice (cubic fluorite for YSZ), the DFT structures used to train the CEs are allowed to relax without symmetry constraints. Therefore, other crystallographic types, achievable through continuous transformation and also able to be mapped back onto the underlying CE lattice (e.g., tetragonal onto cubic), are implicitly represented within the CE. This is important when considering results where real materials such as YSZ have mixed phases and T-dependent phase transitions (e.g., cubic→tetragonal→monoclinic). In the case of ionic solids such as YSZ, long-range electrostatic interactions are explicitly represented and subtracted from the total energy, leaving the CE to fit the shorter range interactions. Electrostatic interactions are then added back into the total-energy expression to reconstruct a structure's 0 K energy.

A crossvalidation (CV) score [Eq. (2)] is often used to evaluate the predictive error of the cluster expansion. The CV score, analogous to a normal root-mean-square error, is calculated by comparing the difference between each *ab initio* calculated energy E_i and the associated predicted CE energy $E(\sigma)$ found using the $N-1$ remaining structures as the CE training set. Achieving a CE with a CV score low in comparison to the temperature regime of interest (e.g., <25 meV per lattice site at ~ 300 K) gives a reliable first look at the general predictive power of the CE,

$$\mathrm{CV} = \left\{ \frac{1}{N} \sum_{i=1}^{N} [E_i - E(\sigma)]^2 \right\}^{1/2}. \tag{2}$$

As the fitted cluster coefficients [Eq. (1)] contain values that represent energy contributions from atomic interactions, inconsistent atomic interaction data lead to inconsistent CE energy predictions and thus a large CV score. One can often reduce inconsistencies by removing all structures with energies high above the ground state within the set of structures with the same concentration but different configurations, here defined as a concentration set. A check of these excluded high-energy structures against their DFT calculated energies often reveals, however, that the excluded structures are predicted as ground states by the CE. The inconsistencies within atomic interactions can also be diminished by limiting formal charge values, $\rho(\sigma)$, to close to zero [Eq. (3)], where oxidation states of Zr^{3+}, Y^{2+}, and O^{2-} are assigned and/or limiting the training structures used to construct the CE to the concentration range of most interest (e.g., $x<0.16$ in this work). A rapidly converging short-range cluster expansion is easy to construct over such a narrow concentration range whereas obtaining a similar accuracy over a wider concentration range necessitates far longer range interactions,

$$\rho(\sigma) = 2\delta/\mathrm{f.u.}, \tag{3}$$

where $(\mathrm{Zr}_{1-x}\mathrm{Y}_x)\mathrm{O}_{2-x/2-\delta}$. The danger implicit in this method becomes evident upon lattice Monte Carlo (LMC, see below) equilibration while the overall composition of a structure may lie within the range of a restricted CE (e.g., $x=0.08$ or 8% Y), extended domains of the material may contain high concentrations of the dopant or defect (e.g., containing 66% Y), locally transgressing the CE model's boundaries. Under such conditions, CE-predicted energies produced by concentration or energy-range restricted CEs cannot be trusted, as was found in the case of YSZ when initially using a yttrium concentration restricted CE.

An adaptive cluster expansion with a formal-charge dependence [Eq. (4)] can be introduced to mitigate the difficulty present when cluster expanding systems with widely varying atomic interactions across concentration space and variable stoichiometry,

$$E(\sigma) = \sum_{\alpha} m_{\alpha} (J_{\alpha} + J'_{\alpha} \rho(\vec{\sigma})) \langle \varphi_{\alpha}(\vec{\sigma}) \rangle. \tag{4}$$

Here J'_α are additional charge-dependent variational coefficients and $\rho(\sigma)$ is the formal charge in the fitted structure. The introduction of charge-dependent terms does not fundamentally change the CE formalism; the ECI are simply expanded into linear functions of the formal charge. One can imagine creating several YSZ CEs, each for $0 \le x \le 1$ of Eq. (3) but various values of δ. Each CE would be independently valid for structures off the appropriate δ. The adaptive CE connects the hypothetical independent CEs into a single continuous mapping; the expansion basis itself, $\varphi_\alpha(\sigma)$, remains unchanged. One could similarly create an adaptive CE with concentration dependence.[17] Practically, the adaptive CE allows variation in the energy contribution of each atomic interaction across formal-charge or concentration space. Consequentially, using higher order ECI terms (e.g., $J\Box_\alpha$) can significantly decrease the need for larger (triplet, quartet, etc.) and longer range clusters as well as reducing the need to explicitly remove long-range electrostatic energies before cluster expansion construction. For YSZ, the modified CE better represents structural energies, leading to substantially enhanced predictive precision (i.e., lower CV scores) at a modest increase in computational effort. This formalism was primarily developed in the present context to aid in ground-state structure searches of small, ordered structures.

Once an adequate CE is constructed, it must be remembered that the CV score is an averaged value; entire concentration spaces within the modeled system can be poorly fit while the overall CV score remains low. This necessitates care in interpretation of any results which include the poorly fit concentration spaces. As it happens, the atomic-level clustering found in YSZ and discussed below provides severe tests for the CE methodology.

When it is determined that long-range interactions are needed, determining the optimal set of included clusters results in a search through 2^N possible solutions, where N is the number of included clusters. Prior work[18] has shown that the search for an optimized solution can be greatly aided by a genetic algorithm fitting scheme. Genetic algorithms use an evolutionary approach to the optimization problem. From the total set of included clusters, a trial set of solutions each composed with a unique subset (genome) of clusters (genes) is drawn from the total set of included clusters. A fitness score, usually the CV score for cluster expansion, is assigned to each genome. If needed, a revised fitness score can augment the CV score with penalties for undesirable fit scenarios such as incorrect ground-state ordering. Subsequent generations are formed by swapping gene sequences between the fittest "parent" genomes or inducing mutations into individual genes to form "children." The process is repeated until an optimized solution is obtained. For a simple system, genetic algorithms often lead to a single optimized solution from random starting configurations. Complex systems require large genomes and, as genetic algorithms are stochastic, can lead to locally optimized results far from the global optimum: essentially an evolutionary dead end. Thus, several independent "evolutionary startups" are required to ensure a reasonable chance of finding a result near the global minimum. A fundamental assumption in the use of cluster expansions in crystalline systems, that a CE is dominated by the shortest range interactions, can be used to guard the optimization from search regions that often lead to evolutionary dead ends. The genetic algorithm can be initialized using only the shortest range clusters and, as it is seen that the longest range clusters included in the genome enhance the fit, increasingly longer range clusters are included. This method forces a thorough optimization of the dominant short-range clusters.

B. Finite-temperature cluster expansions

1. Vibrational free-energy approach

A cluster expansion fitted to first-principles energies is by construction a $T=0$ energy equation, as discussed above. For this cluster to be used in finite-temperature statistical models, knowledge of cluster coefficient evolution with increasing temperature is needed beyond that implied by Boltzmann statistics on electronic energies. As a reasonable first approximation to finite-T effects on structure, the vibrational free energy can be added to the structural energy expansion.[19] The electronic free-energy contributions can be similarly added to the cluster expansion and would likely be significant in soft phonon or surface systems.[20] In most crystalline systems at normal working temperatures, the structural and vibrational free energies dominate over the electronic free-energy contributions. Interspecies forces, obtained from first-principles calculations on local perturbations of several of the training structures' equilibrium atomic positions at varied cell volumes, are used to obtain interspecies stiffness vs length force equations applicable across concentration space. The vibrational density of states (VDOS) $g(\omega)$ for each calculated training structure is found in the harmonic approximation from the k-space sampled dynamical matrices derived from these force equations applied to each structure's relaxed atomic positions. A Gaussian line shape is applied to transform the VDOS to smooth curves for presentation purposes.

Though a quasiharmonic approximation[21] can be implemented that accounts for thermal expansion by allowing the vibrational modes to be volume dependent, YSZ has low thermal expansion (reported as 10.5×10^{-6} K^{-1} for 8 mol % Y_2O_3 and dropping with increasing Y_2O_3 content[22]). Therefore, the harmonic approximation is considered sufficient in the present context.

The vibrational free energy[23] [Eq. (5)], and other quantities such as the entropy and the specific heat, can be easily determined by standard methods after the determination of the VDOS,

$$F = -3rNk_BT\int \ln\left\{2\sinh\left(\frac{\hbar\omega}{2k_BT}\right)\right\}g(\omega)d\omega. \tag{5}$$

In the present case, the so-called high-temperature limit, for which $T>\theta_{\text{Debye}}$, is used for the vibrational entropy Eq. (6) and free energy,

$$S(T>\theta_{\text{Debye}}) = 3rNk_BT\int\left[1-\ln\left(\frac{\hbar\omega}{2k_BT}\right)\right]g(\omega)d\omega. \tag{6}$$

The calculated vibrational free energies are then mapped onto the original 0 K clusters, resulting in the T-dependent vibrational energy cluster expansion of Eq. (7),

$$J_\alpha(T) = J_\alpha + J_\alpha^{vib}(T). \tag{7}$$

2. Lattice Monte Carlo approach

The finite-T energy cluster expansion is utilized to bridge the atomistic-scale quantum model to a statistical-scale thermodynamic model obtained using LMC algorithms implemented within ATAT. The LMC algorithm is a semigrand canonical ensemble model[24] that allows the concentration of each species to respond to externally imposed chemical potentials as the total number of lattice positions is kept fixed. The LMC algorithm, using the first-principles-derived energy cluster expansion, gives us structurally equilibrated free energy over a range of temperatures and chemical potentials. This approach is particularly well suited to determining optimized nanostructures of thermally equilibrated systems and their associated energies. The LMC grand canonical chemical-potential-energy formulation requires each species' chemical potential as input, which is not generally experimentally known. Though there are several assumptions that can be made to make the problem more tractable (e.g., using the experimental oxygen gas chemical potential to determine oxide oxygen chemical potential and fixing relatively immobile cation concentrations), the main goal of this study was to study dopant/vacancy ordering of set concentrations. Thus, LMC was operated as a canonical ensemble, with fixed concentrations.

LMC equilibrated structures were analyzed primarily using two-body atomic radial distribution functions. Experimental two-body radial distribution functions are found by spectroscopic procedures such as extended x-ray absorption fine structure[25,26] and neutron diffraction,[27] aiding in understanding $g_{ij}(r)$ structural data such as average coordination sphere radii and occupation number of component elements. The distribution of dopants and defects within a structure can be linked to dynamic properties such as diffusion, as in YSZ where oxygen jumps into oxygen vacancies near yttrium are reported to be less likely[28] and in Li_xCoO_3 structures where the number of divacancies is proposed to be directly related to the rate of diffusion.[8] As precise experimental atomic ordering data of nanostructured materials are still difficult to obtain, computationally based theoretical two-body radial structural analysis is an important tool to complement experimental determinations of the coordination and distribution of species.[29–31] A theoretical discrete radial distribution function is simply obtained here by analyzing the thermally equilibrated LMC configurations, as an average over all equivalent sites. Of further interest is to determine how defects and dopants associate in groups. There have been suggestions that the association of defects with dopants influences aging and ionic conduction mechanisms:[11] these associates can simply be enumerated and visualized from equilibrated LMC configurations.

The theoretical distributions developed here are necessarily discretized as LMC is a lattice model in which only lattice occupations, and not lattice locations, are sampled; site relaxation energies are implicitly built into the clusters. Two-body distributions are computed by averaging the species occupation of neighbor sites of all equivalent sites, giving a description of local distributions and coordination numbers.

III. RESULTS AND DISCUSSION

A. Density-functional calculations

The YSZ CE model was initialized in a cubic fluorite structure. While in reality YSZ is a variable phase material (monoclinic, tetragonal, and cubic) for concentrations less than 10 mol % Y_2O_3 at 0 K and concentrations less than 8 mol % Y_2O_3 at ~1250 K,[32] the cubic fluorite structure, with its induced oxygen vacancies, is the enabler of fast ionic diffusion and thus is the crystallographic structure of main interest over the Y concentration range studied. As mentioned previously, DFT calculated structures used to train the CEs are allowed to relax without geometric constraint. Therefore other crystal structures that can be mapped onto a cubic lattice via continuous deformations can be and are included within this framework as well. The structural training sets, consisting of periodic supercell structures, were relaxed using plane augmented wave pseudopotentials and the local-density approximation (LDA) employed within the Vienna *ab initio* simulation package (VASP).[33] More complex DFT functionals such as the generalized gradient approximation (GGA) often predict material properties such as bond lengths, magnetic properties, and band gaps more in accord with experiment as compared to the simple LDA. Since the *relative energies* of related structures are all that is necessary for the success of an accurate YSZ energy cluster expansion, it was deemed unnecessary to use the more complex and computationally GGA throughout. As a test of this choice, 20 structures within three concentration sets were also calculated using the PW91 GGA functional, resulting in little or no reordering of the relative formation energies within each concentration set, relative to the LDA results. Comparisons with experimental ordering data also suggest the adequacy of the LDA approximation for present purposes.

Electronic density of states

Electronic partial densities of states for cation and anion distributions were calculated for the optimized stoichiometric ground states of ZrO_2, 33YSZ, 66YSZ, and Y_2O_3 in order to detect any major changes in electronic structure with composition (Fig. 1). In the LDA potential used for most of the thermodynamic analyses, one finds a predicted insulating structure for all compositions, with a band gap of 3–4 eV. The upper valence band, with strongly overlapping bonding oxygen 2*sp* and metal states is of ~5 eV in width, varying relatively little with composition. Unoccupied antibonding cation and oxygen-hole states form the first conduction band, of width ~2 eV, while the end-member ZrO_2 shows a somewhat broader two-subband structure. LDA is well known to underestimate band gaps: the experimental gap for ZrO_2 is 3–5 eV (Ref. 34 and references therein). In the case of considerable deviation from stoichiomety, with large oxygen vacancy excess, we expect that defect states would appear in the gap region.

B. Cluster expansion strategy

Initial results using a restricted CE ($x<0.33$ and $\delta=+/-0.08$) showed highly ordered domains with significant yttrium and oxygen vacancy content outside the restricted CE boundaries. Therefore the model used here was expanded to include yttrium concentrations from $0\leq x\leq 1$. Several small cubic structures with concentration equal to Y_2O_3 were calculated rather than the full 80 atom bixbyite structure to help characterize the "intrinsic vacancies" of the material and save computational cost. All structures within the Y_2O_3 set were well fit. Formal charge deviation from neutrality, δ, was kept within $+/-0.17$ and all high-energy structures calculated were included in the training set.

A total of 699 training structures were generated to fit 595 clusters from which the genetic algorithm selected an optimized set of 169 clusters for subsequent use. This resulted in a structural energy CV score of 18 meV per lattice site with correct (i.e., identical to LDA) CE-predicted ground-state ordering within a tolerance equal to the CV score. A vibrational

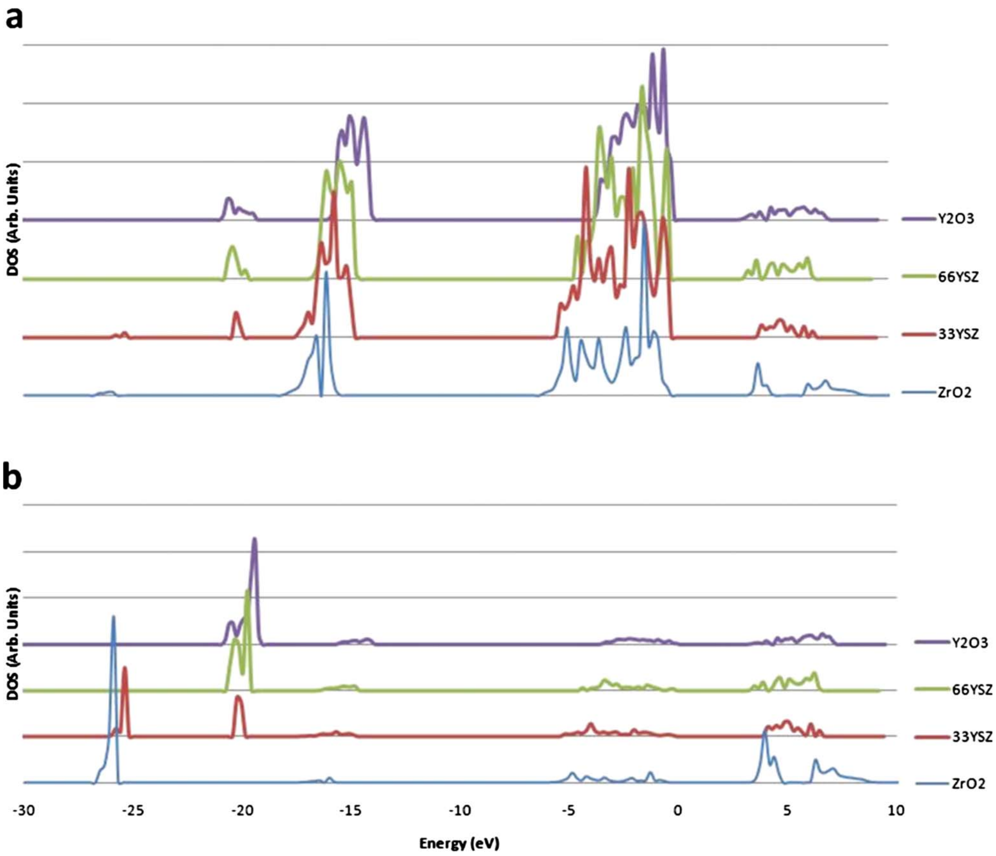

FIG. 1. (Color online) Partial density of states of (a) oxygen and (b) cations for four stoichiometric ground states with various Y content.

free-energy cluster expansion was calculated using the original 595 clusters, of which 155 were retained, with average CV score of 3 meV per lattice site. Given the high temperatures involved in YSZ electrolyte applications (usually >1000 K), these CV scores are considered adequate for analysis of both structural and vibrational properties.

C. Dopant/vacancy ordering

LMC was used to calculate the ordering of yttrium dopants and oxygen vacancies for randomized, stoichiometric initializing structures with Y concentrations between $x=0.03$ and 0.16. The typical model used a $24\times24\times24$ periodic LMC cell (~ 8 nm on a side) containing 41,472 lattice positions, including oxygen vacancies which were treated mathematically as a unique chemical species. Initial runs carried out on an extended $30\times30\times30$ periodic cell did not yield significant additional/different local ordering information. Thus the smaller cell was deemed sufficient for subsequent calculations. Reported results are the average of several randomized trial structures at each surveyed yttrium concentration equilibrated at 1200 K. The following nomenclature is used: yttrium concentration will be given as a number before YSZ; e.g., stoichiometric YSZ with $x=0.08$ and $\delta=0$ from Eq. (3) will be listed as 8YSZ.

The cluster coefficients, J_α, of Eq. (1) hold all the system structural energy information, implicitly including relaxation data. At this stage of CE methodology development, lattice relaxation information cannot be extracted back from the CE for explicit use, though such a method could possibly be derived from an extension of the previously developed tensorial cluster expansion.[14] This constraint requires the two-body distribution functions used to describe atomic ordering to be discrete and dimensionless functions ordered by coordination shell. In this description, each lattice location in a focus' shell is equidistant from the focus lattice location. Each shell's type is described by its typical occupation, either anion or cation. For instance, the Y-Vac interaction is described as a focus yttrium atom surrounded by a series of anion shells with vacancy occupancy at discrete, increasing radial distances. In the case of the Y-Y interaction, the first

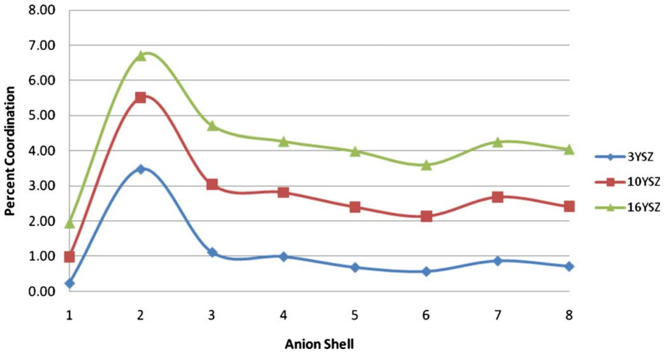

FIG. 2. (Color online) Not-aged Y-Vac shell ordering within ~ 1 nm radius of all Y sites for various Y concentrations.

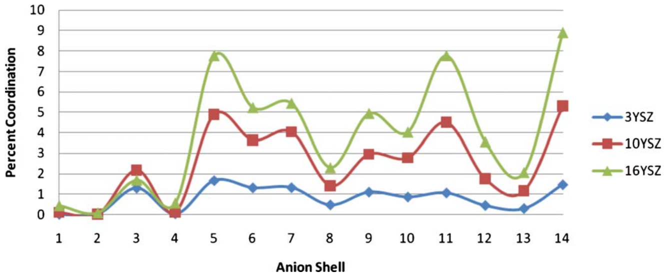

FIG. 3. (Color online) Not-aged Vac-Vac shell ordering within ~1 nm radius of all vacancy sites for various Y concentrations.

cation shell is synonymous with the second coordination sphere surrounding an yttrium atom.

1. Sequential ordering model and aging

Anions in YSZ migrate at a much faster rate than cations. Therefore, to simulate the initial configuration of bulk YSZ materials immediately after synthesis and sintering, the randomly generated structures were first equilibrated with the cation lattice positions held fixed. In the following this model is referred to as “not aged.” This model ignores the limited cation ordering that is expected to take place upon syntheses. Ordering, as reported here, is often represented as a percent occupancy (% occ) of a given coordination shell.

Results for 10YSZ correspond well to prior finite-*T* experimental data. In particular, the CE derived atomic ordering results replicate two major conclusions from previous studies: (i) the average oxygen coordination of Zr’s first anion shell (here calculated as 7.79) is less[35,36] than that of Y (7.92), which favors full eightfold oxygen coordination.[35,36] (ii) Vacancies associate more favorably as second anion shell neighbors[4] with Y dopants (5.5% occ) as compared to the first anion shell neighbors (1.0% occ). Full results from the not-aged model are reported in Figs. 2 and 3.

Visual inspection and Vac-Vac ordering results (Fig. 3) of the not-aged structures across all concentration ranges shows the formation of extended but diffuse vacancy aggregations within the volume. As the Y atoms are randomly distributed, there exist domains with increased average Y content. The vacancy aggregations apparently follow these increased Y density domains. Vacancy aggregation has been suggested by previous theoretical[37] and experimental work,[27] in particular, third and sixth anion shell Vac-Vac orderings. Unlike past work, however, the present results show significant fifth anion shell Vac-Vac ordering. Other studies of longer than sixth shell Vac-Vac and second shell Y-Vac ordering are not readily available for comparison.

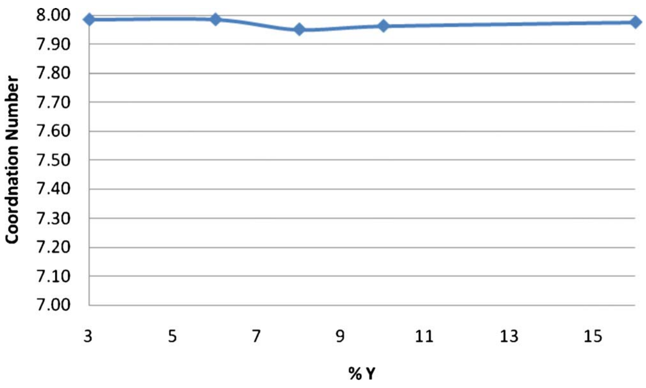

FIG. 4. (Color online) Aged Y-O shell coordination versus Y content.

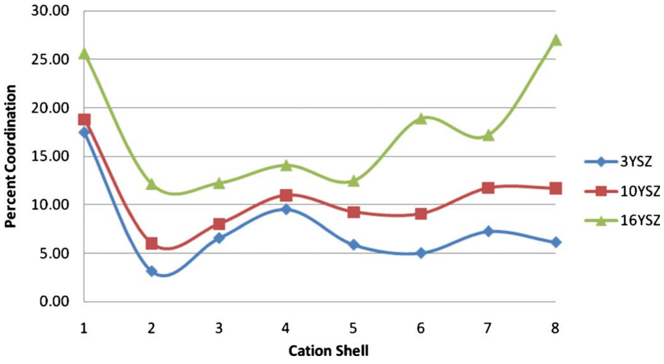

FIG. 5. (Color online) Aged Y-Y shell ordering within ~1 nm radius of all Y sites for various Y concentrations.

2. Aged YSZ

“Aging,” in contrast to not-aged modeling, is simulated by allowing *both* anions and cations to thermally equilibrate. Equilibration was performed allowing only nearest-neighbor hops starting from the previously anion-equilibrated, not-aged structures. While this type of modeling has no time scale, trajectories of dopant migration can be observed.

In good agreement with experiment,[25] the first anion shell Y-O distribution resists deviation from full YO_8 coordination (Fig. 4); dopants with atomic radii larger than Zr, such as Y, maintain their local environment independent of phase. In comparison to the not-aged model, longer range Y-Vac ordering is evident as well as a significantly enhanced seventh shell Vac-Vac ordering. Y-Vac ordering also seems approximately constant below 10YSZ. It has to be noted that Y-Y ordering has a great influence on the exact nature of long-range Vac-Vac ordering. Thus any change in the Y-Y order would be reflected in an associated change in the Vac-Vac ordering. Standard deviations for fifth, seventh, 11th, and 14th Vac-Vac shells are exceptionally high, unlike those in the not-aged model. Y-Y ordering standard deviations are

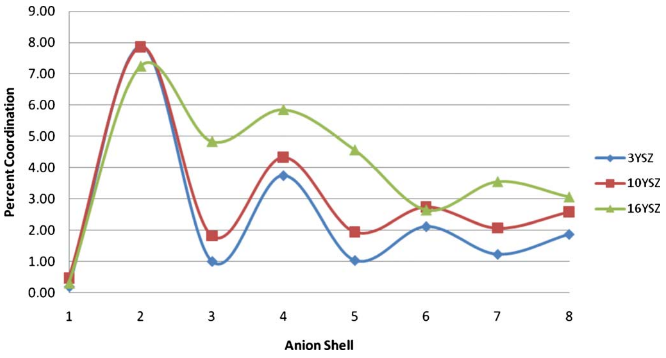

FIG. 6. (Color online) Aged Y-Vac shell ordering within ~1 nm radius of all Y sites for various Y concentrations.

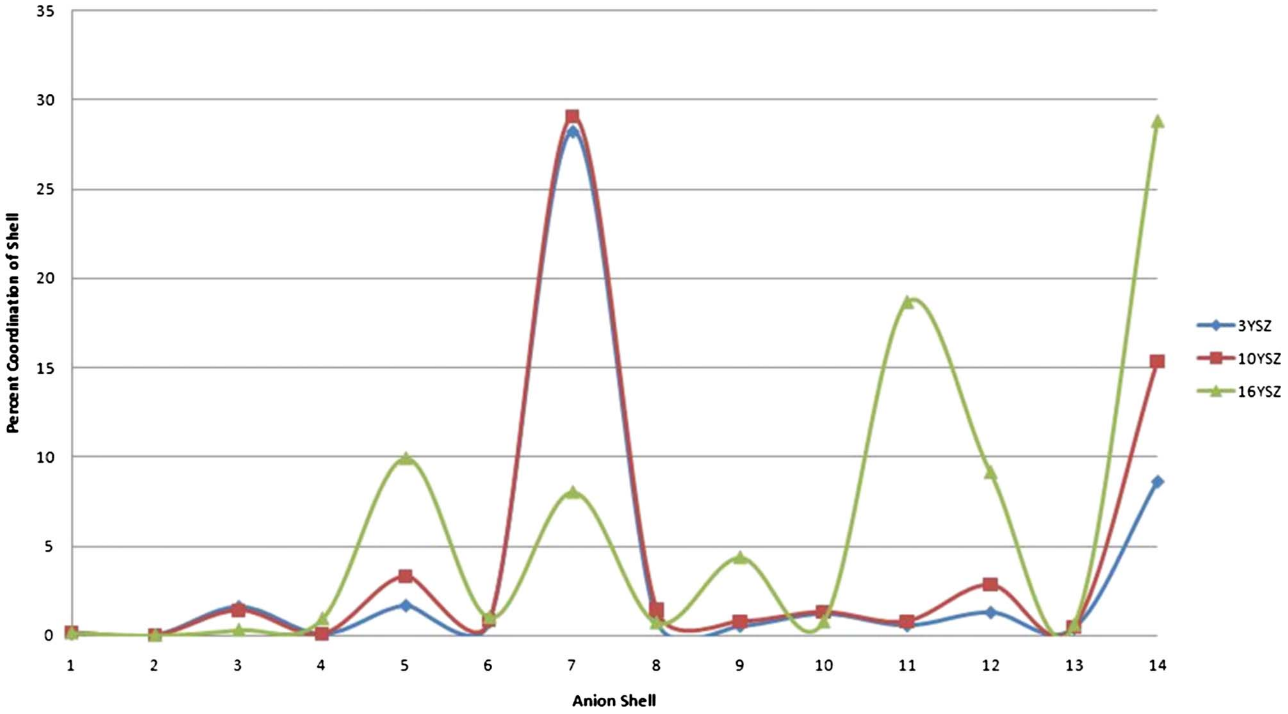

FIG. 7. (Color online) Aged Vac-Vac shell ordering within ~1 nm radius of all vacancy sites for various Y concentrations.

also high. These results suggest that the distribution of Y in the randomly generated initializing structures is important to the detailed outcome of both Y-Y and Vac-Vac orderings but not significantly to Y-Vac ordering. Full results across Y concentration are reported in Figs. 5–7.

Aged model equilibration of both cations and anions yields Y-rich nanodomains with oxygen vacancies aggregating in and around them. Whereas not-aged (anion) equilibration showed large aggregations of vacancies distributed throughout the volume, aged equilibration shows these vacancy aggregations prefer association solely around the Y-rich aggregates.

There are several possible explanations for the experimental ionic conductivity aging effects in YSZ, referred to previously. These can be grouped into several classes. (i) Domain phase transformations revert some cubic YSZ back to less favorable monoclinic and tetragonal phases.[38] (ii) Ionic conduction degrades due to dopant and vacancy clustering. Any ordering that stabilizes vacancies, via yttrium trapping or vacancy-vacancy ordering, lowers vacancy mobility. (iii) Dopant segregation into grain boundaries depletes necessary stabilizing yttrium from the bulk regions, forcing phase reversion (a subset of option 1). (iv) At low dopant levels (<9 mol % Y_2O_3), association of vacancies with dopants into dipoles (Vac-Y) and tripoles (Y-Vac-Y), which immobilize vacancies, is limited. With aging, these defect associates form, degrading the ionic conductivity. At higher dopant levels, the defect associates have already reached a saturation point, so no further deleterious aging effects are noticed.[11]

Appreciable increases in oxygen diffusion around 8YSZ and sharp decreases in oxygen diffusion with aging for concentrations <9 mol % yttria suggest that the diffusion rate is not a simple function of the number of available vacancies. Not-aged conduction peaks are normally attributed to simultaneously reaching full cubic stabilization at and above 8 mol % Y_2O_3 and having lower diffusion-hindering Y-Vac ordering than, say, 10 mol % Y_2O_3 (Fig. 2). The anomalous aging effects have yet to be satisfactorily explained.

Current aged model results seem to contradict hypothesis (iv) as aging seems to decrease the incidence of first shell Y-Vac associates for all surveyed concentrations of Y. First and second Y-Vac shell ordering is nearly identical below 10YSZ in the aged model (Fig. 6). While second shell Y-Vac ordering increases for both 8YSZ and 10YSZ, first shell Y-Vac ordering decreases to almost zero due to the rearrangement of the Y-Y ordering upon aging, suggesting that Y-Vac-Y tripole formation is not a great degrader of conduction. Near Y-Vac and long-range V-Vac ordering does increase overall for 8YSZ, in support of hypothesis (ii). There is some reported limited degradation of 10YSZ at ~1200 K (Ref. 11) experimentally, though not nearly to the extent of 8YSZ. Therefore, results here suggest that increased trapping is likely to exist but in the context of this study, it cannot be

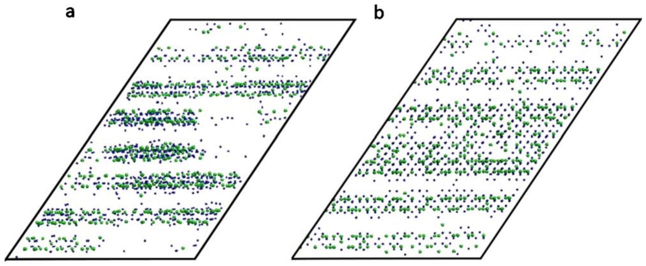

FIG. 8. (Color online) Cross section of planar (a) 8YSZ and (b) 10YSZ structures in the aged model. 24×24×24 cell equilibrated at 1200 K. Blue: equilibrated Y and green: equilibrated O vacancies.

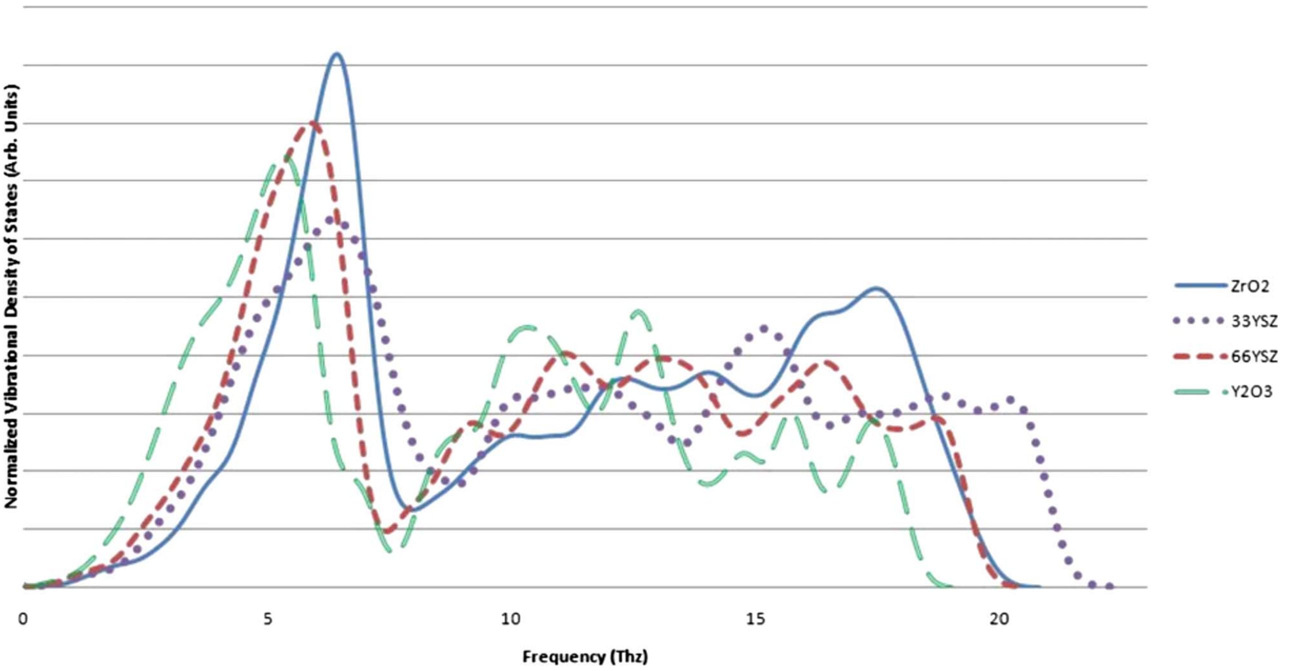

FIG. 9. (Color online) Vibrational density of states for four stoichiometric ground states with various Y content.

determined to what extent it influences conduction degradation. There is likely still another cause for the sharp drop in ionic conduction for structures less than 9 mol % Y_2O_3.

Visual inspection of the aged model shows that in both 8YSZ and 10YSZ, two different types of equilibrated structures can result: (i) small aggregates of Y (4–6 atoms) are distributed unevenly throughout the cell volume. (ii) Y form diffusely disordered planes separated by ∼1 nm gaps (Fig. 8).

These two equilibrated structure types, for both 8YSZ and 10YSZ, differ in energies less than is resolvable within our CE model (∼0.5 meV per lattice site). While the presence of long-range, periodic superstructures has not been previously been suggested in YSZ materials, it has been seen that where significant infinite-range interactions exist, such systems can form.[39]

Unlike 10YSZ, both equilibrated configurations of 8YSZ leave domains of material (up to 3–5 nm on a side) almost entirely devoid of Y and Vac. Both experiment[26] and theory[40] have previously led to suggestions that the vacancy distortions of the anion coordination sphere around Zr appearing as $ZrO_8 \rightarrow ZrO_7$, causing inefficient “packing,” give rise to lattice expansion and thus the stabilization of the global cubiclike lattice symmetry. Thus, local atomic ordering, needing to accommodate the foreign ZrO_7 polyhedra, departs from the fluorite structure. Therefore, it is feasible that the depleted domains could either have a phase stabilized by the surrounding vacancy-distorted lattice or phase revert back to either tetragonal or monoclinic. Regardless, as vacancies preferentially stay near Y atoms, domains depleted of Y and Vac function as blockades, forcing migrating oxygen ions to make a time-consuming detour around the affected domains. This result, supporting hypotheses (i), seems to be the primary explanation for the ionic degradation for 8YSZ as compared to 10YSZ, and such degradation would be further aggravated with dopant segregation to grain boundaries [hypothesis (iii)].

D. Vibrational properties

1. Vibrational DOS

One can see the evolution of the vibrational density of states as Y content is increased from 0% to 100% in Fig. 9. Comparison to previous theoretical work[41] suggests that cations are the primary participants of low-frequency modes (5–6 THz), mixed cation-anion participation in middle-frequency modes (7–15 THz), and high-frequency modes (15–23 THz) primarily resulting from anion vibrations. Notably, the magnitude of the 33YSZ cation-cation modes sig-

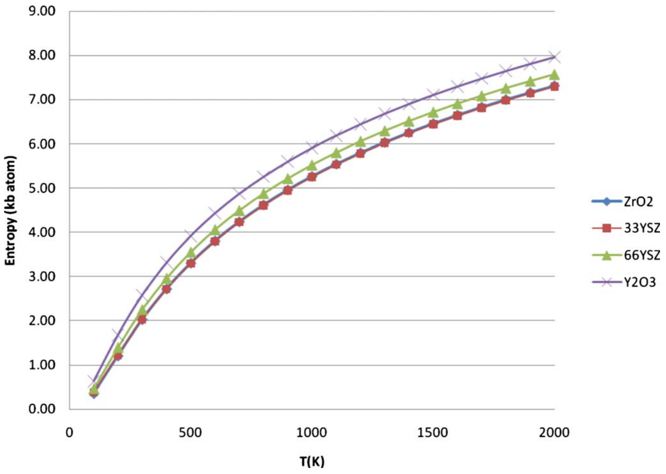

FIG. 10. (Color online) Vibrational entropy for four stoichiometric ground states with various Y content. The ZrO_2 entropy values are degenerate with those of 33YSZ.

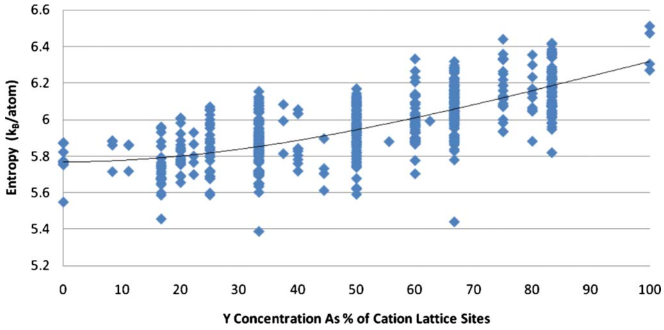

FIG. 11. (Color online) Vibrational entropy at 1200 K versus Y concentration for all calculated structures. A median curve is drawn.

nificantly decreases compared to pure zirconia and is accompanied by an increase in high-frequency modes. This would indicate that delocalized, low-frequency modes are disrupted by vacancy formation, creating localized, high-frequency modes. In absence of significant experimental data for comparison, no further detailed analysis is warranted.

2. *Vibrational entropy*

Vibrational entropy, which counts the number of vibrational modes accessible to the individual atoms at a given T, is reported in Fig. 10. Vibrational entropy for YSZ structures from pure zirconia to at least 33YSZ is calculated to be essentially constant with respect to Y content. Entropies differences of same concentration structures are qualitatively similar to differences reported in literature (Ref. 19 and references therein). Vibrational entropy tends to increase with both increasing Y and vacancy content (Figs. 11 and 12). Whereas any increase in vibrational entropy with composition has no effect on phase stability, these calculations suggest that entropic contributions to the free vibrational energy are either level or very slowly rising for concentrations $<20\%$ Y and $<5\%$ Vac.

Vibrational entropy changes are surveyed with alternatively fixed vacancy (Fig. 13) and Y (Fig. 14) concentrations around stoichiometric 33YSZ. In both cases, entropy is increased when the material is off-stoichiometry. This would imply that vibrational entropy, at relatively low Y concentrations, favors charge imbalanced domain formation.

FIG. 12. (Color online) Vibrational entropy at 1200 K versus vacancy concentration for all calculated structures. A median curve is drawn.

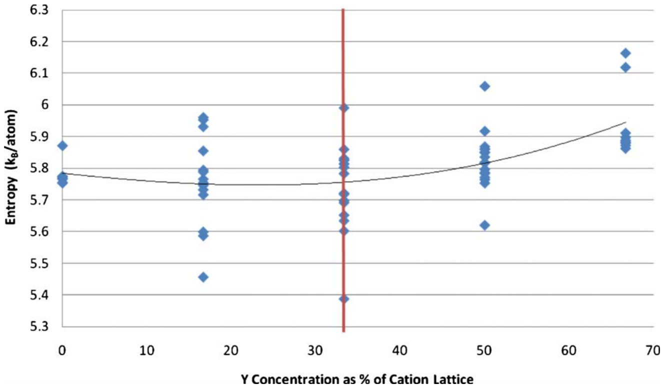

FIG. 13. (Color online) Vibrational entropy at 1200 K versus Y concentration for all structures with 8.3% vacancies on the anion lattice; 33% Y content is stoichiometric (red vertical line). A median curve is drawn.

3. *Vibrational free energy*

Vibrational free energy (F) per lattice position over a temperature range of $0<T<2000$ K for each DFT calculated structure was found. Figure 15 shows the how vibrational free energy develops with temperature for four stoichiometric ground states. The pure ZrO_2 material is unfavored at low temperature but becomes increasingly favored as temperature increases. Strikingly, as temperature increases past $\sim$1000 K, pure ZrO_2 and Y_2O_3 structures become favorable over mixed concentration ordered states. Figures 16 and 17 further suggest that stoichiometric structures at high T are not strongly preferred. It appears that vibrational free energy favors phase separation into pure ZrO_2 and Y_2O_3 at high temperatures whereas structural energy favors separation into pure ZrO_2 and mixed phases.

IV. CONCLUSIONS

The lattice-site-based cluster energy expansion scheme was extended by inclusion of charge-dependent variables, allowing a more efficient procedure dominated by short-range terms, at a modest increase in computational effort. Exclusion of charge-dependent terms leads to larger expan-

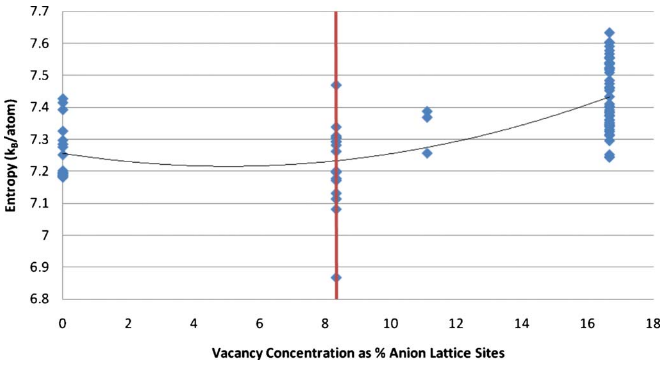

FIG. 14. (Color online) Vibrational entropy at 1200 K versus vacancy concentration for all structures with 33% Y on the cation lattice; 8.3% vacancy content is stoichiometric (red vertical line). A median curve is drawn.

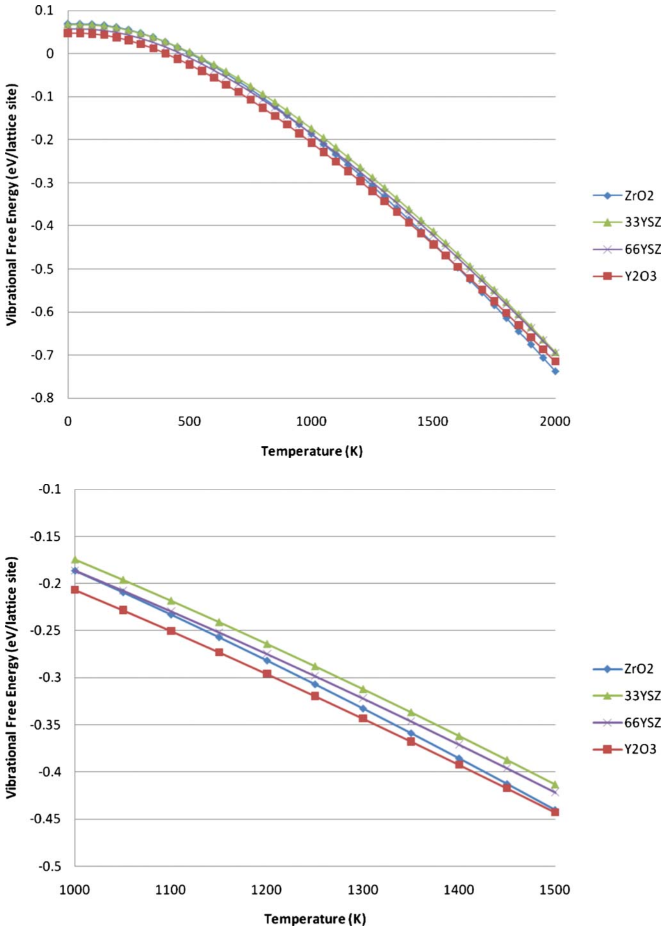

FIG. 15. (Color online) Vibrational free energy per lattice position versus T for four stoichiometric ground states with various Y content. Vibrational free energy: expanded view of Fig. 15.

sions with longer range interactions needed to achieve a given level of precision in fitting first-principles data. A genetic algorithm was developed which facilitated the construction of a DFT derived, temperature-dependent CE for the free energy of $(Zr_xY_{1-x})O_{2-x/2+\delta}$. The genetic algorithm proved to be orders of magnitude more rapid in locating favorable expansions compared to straightforward cluster sampling. The resulting CEs were coupled to a lattice Monte Carlo method from which statistical average electronic and lattice properties were obtained.

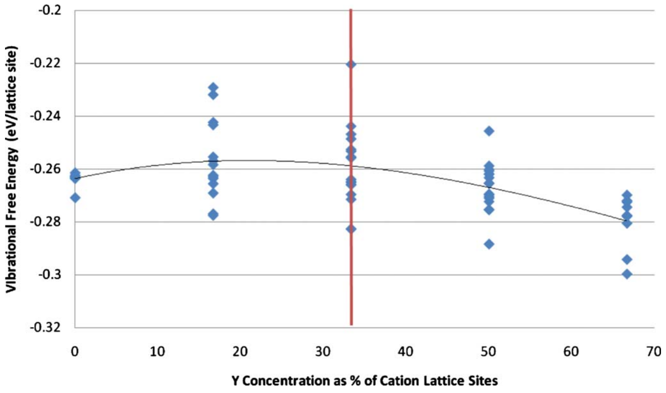

FIG. 16. (Color online) Vibrational free energy (F) at 1200 K versus Y concentration for all structures with 8.3% vacancy on the anion lattice; 33% Y content is stoichiometric (red vertical line). A median curve is drawn.

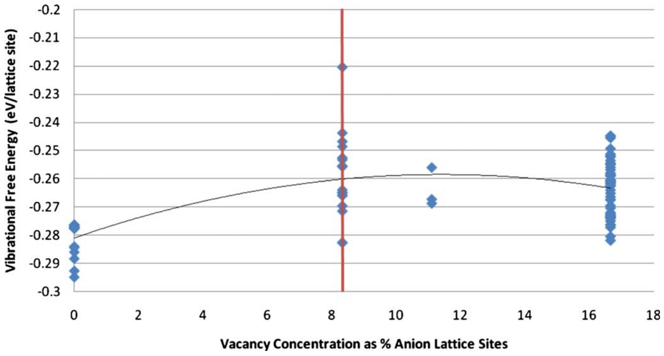

FIG. 17. (Color online) Vibrational free energy (F) at 1200 K versus vacancy concentration for all structures with 33% Y on the cation lattice; 8.3% vacancy content is stoichiometric (red vertical line). A median curve is drawn.

Concerning electronic properties. Densities of states show a band gap ranging from ~3 to 4 eV across the YSZ concentration range. This result compares favorably with existing experimental band-gap data which suggests a band gap of 3–5 eV is to be expected.

Concerning atomic-scale ordering, principal findings. (i) Calculated two-body radial distributions of YSZ of a range of Y concentrations $(0 < Y < 16\%)$ show good agreement with previous experimental and theoretical results. (ii) A "not-aged" anion-relaxed YSZ model shows diffuse oxygen-vacancy aggregations. (iii) A fully equilibrated "aged" YSZ model shows formations of Y-rich aggregates which attract and, and presumably, trap oxygen vacancies. (iv) Present results suggest that thermal aging leads to the increase in both yttrium and vacancy aggregation. Such aggregations in aged 8YSZ deplete both Y and oxygen vacancies from sizable domains of material. This depletion was not observed in aged 10YSZ structures. Depleted nanodomains could possibly phase revert to tetragonal or monoclinic phases and present detours for migrating oxygen ions, increasing diffusion path lengths.

Concerning vibrational properties. Using a harmonic approximation, high-T vibrational free-energy model derived from interspecies stiffness vs length force equations, one finds: (i) vibrational free-energy comparison of a range of stoichiometric structures shows phase separation into pure ZrO_2 and Y_2O_3 at temperatures greater than 1000 K is favored. (ii) Vibrational free-energy scans across dopant/defect space show that for a given dopant concentration, the formation of nonstoichiometric structures is favored.

The methodology described in this work and applied to YSZ shows good agreement with past experimental and theoretical works where they are comparable and throws light upon the connection between atomic ordering and ionic conduction in YSZ. Such agreement gives confidence that these atomic-ordering CE methods should be directly extensible to more complex perovskite-structure ionic and electronic conductors.

ACKNOWLEDGMENTS

Work supported by the U.S. Department of Energy, Basic Energy Sciences, under Award No. DE-FG02-05ER46255, by the U.S. National Science Foundation under Grant No. DMR-0953378, and by Teragrid Resources provided by NCSA under Grant No. DMR050013N.

---

*Corresponding author; don-ellis@northwestern.edu

[1] http://www.fossil.energy.gov/programs/powersystems/fuelcells/

[2] *Science and Technology of Zirconia*, Advances in Ceramics, edited by A. H. Heur and L. W. Hobbs (The American Ceramic Society, Columbus, OH, 1981).

[3] M. Kilo, C. Argirusis, G. Borchardt, and R. A. Jackson, Phys. Chem. Chem. Phys. **5**, 2219 (2003).

[4] R. Devanathan, W. J. Weber, S. C. Singhal, and J. D. Gale, Solid State Ionics **177**, 1251 (2006).

[5] P. S. Manning, J. D. Sirman, R. A. DeSouza, and J. A. Kilner, Solid State Ionics **100**, 1 (1997).

[6] A. van de Walle and G. Ceder, J. Phase Equilib. **23**, 348 (2002).

[7] A. Predith, G. Ceder, C. Wolverton, K. Persson, and T. Mueller, Phys. Rev. B **77**, 144104 (2008).

[8] A. Van der Ven, G. Ceder, M. Asta, and P. D. Tepesch, Phys. Rev. B **64**, 184307 (2001).

[9] A. Van der Ven, J. C. Thomas, Q. C. Xu, B. Swoboda, and D. Morgan, Phys. Rev. B **78**, 104306 (2008).

[10] A. van de Walle and D. E. Ellis, Phys. Rev. Lett. **98**, 266101 (2007).

[11] C. C. Haering, A. Roosen, and H. Schichl, Solid State Ionics **176**, 253 (2005).

[12] A. P. Predith, *Computational Studies of Cation and Anion Ordering in Cubic Yttria Stabilized Zirconia* (Massachusetts Institute of Technology, Cambridge, MA, 2006).

[13] P. D. Tepesch, *Atomistic Modeling of Ceramic Materials: Predicting Crystal Structures, Thermodynamic Properties, and Diffusion Behavior* (Massachusetts Institute of Technology, Cambridge, MA, 1996).

[14] A. van de Walle, Nature Mater. **7**, 455 (2008).

[15] J. M. Sanchez, F. Ducastelle, and D. Gratias, Physica A **128**, 334 (1984).

[16] A. van de Walle, M. Asta, and G. Ceder, CALPHAD: Comput. Coupling Phase Diagrams Thermochem. **26**, 539 (2002).

[17] L. G. Ferreira, L. K. Teles, J. R. Leite, and L. M. R. Scolfaro, Phys. Status Solidi C **1**, S198 (2004).

[18] G. L. W. Hart, V. Blum, M. J. Walorski, and A. Zunger, Nature Mater. **4**, 391 (2005).

[19] A. van de Walle and G. Ceder, Rev. Mod. Phys. **74**, 11 (2002).

[20] N. M. Harrison, X. G. Wang, J. Muscat, and M. Scheffler, Faraday Discuss. **114**, 305 (1999).

[21] A. A. Quong and A. Y. Liu, Phys. Rev. B **56**, 7767 (1997).

[22] H. Hayashi, T. Saitou, N. Maruyama, H. Inaba, K. Kawamura, and M. Mori, Solid State Ionics **176**, 613 (2005).

[23] A. A. Maradudin, E. W. Montroll, and G. H. Weiss, *Theory of Lattice Dynamics in the Harmonic Approximation*, 2nd ed. (Academic Press, New York, 1971).

[24] M. E. J. Newman and G. T. Barkema, *Monte Carlo Methods in Statistical Physics* (Clarendon Press, Oxford, 1999); K. Binder and D. W. Heermann, *Monte Carlo Simulation in Statistical Physics* (Springer-Verlag, New York, 1988); B. Dünweg and D. P. Landau, Phys. Rev. B **48**, 14182 (1993); M. Laradji, D. P. Landau, and B. Dünweg, *ibid.* **51**, 4894 (1995).

[25] P. Li, I. Wei Chen, and J. E. Penner-Hahn, Phys. Rev. B **48**, 10074 (1993).

[26] P. Li, I. W. Chen, and J. E. Pennerhahn, J. Am. Ceram. Soc. **77**, 118 (1994).

[27] J. P. Goff, W. Hayes, S. Hull, M. T. Hutchings, and K. N. Clausen, Phys. Rev. B **59**, 14202 (1999).

[28] Y. Yamamura, S. Kawasaki, and H. Sakai, Solid State Ionics **126**, 181 (1999).

[29] G. E. Rush, A. V. Chadwick, I. Kosacki, and H. U. Anderson, J. Phys. Chem. B **104**, 9597 (2000).

[30] P. Ghigna, M. Di Muri, and G. Spinolo, J. Appl. Crystallogr. **34**, 325 (2001).

[31] E. Curis and S. Benazeth, J. Synchrotron Radiat. **12**, 361 (2005).

[32] R. H. J. Hannink, P. M. Kelly, and B. C. Muddle, J. Am. Ceram. Soc. **83**, 461 (2000).

[33] G. Kresse and J. Hafner, Phys. Rev. B **49**, 14251 (1994); **47**, 558 (1993); G. Kresse and J. Furthmuller, Comput. Mater. Sci. **6**, 15 (1996); Phys. Rev. B **54**, 11169 (1996).

[34] D. Ciuparu, A. Ensuque, G. Shafeev, and F. Bozon-Verduraz, J. Mater. Sci. Lett. **19**, 931 (2000).

[35] C. R. A. Catlow, A. V. Chadwick, G. N. Greaves, and L. M. Moroney, J. Am. Ceram. Soc. **69**, 272 (1986); R. B. Neder, F. Frey, and H. Schulz, Acta Crystallogr., Sect. A: Found. Crystallogr. **46**, 799 (1990).

[36] A. Baudry, P. Boyer, and A. L. Deoliveira, Hyperfine Interact. **10**, 1003 (1981); J. Phys. Chem. Solids **43**, 871 (1982); J. A. Gardner, H. Jaeger, H. T. Su, W. H. Warnes, and J. C. Haygarth, Physica B & C **150**, 223 (1988); M. Forker, U. Brossmann, and R. Wurschum, Phys. Rev. B **57**, 5177 (1998).

[37] A. Bogicevic and C. Wolverton, Phys. Rev. B **67**, 024106 (2003).

[38] T. Yamada, T. Fukui, Y. Kodera, and H. Matsubara, Ceram. Trans. **71**, 453 (1996); *Proceedings of the Third European Solid Oxide Fuel Cell Forum*, edited by P. Stevens (European SOFC Forum, Oberrohrdorf, Switzerland, 1998), pp. 171–178; I. R. Gibson, G. P. Dransfield, and J. T. S. Irvine, J. Eur. Ceram. Soc. **18**, 661 (1998).

[39] S. Bärthlein, E. Winning, G. L. W. Hart, and S. Müller, Acta Mater. **57**, 1660 (2009).

[40] S. Fabris, A. T. Paxton, and M. W. Finnis, Acta Mater. **50**, 5171 (2002).

[41] P. K. Schelling and S. R. Phillpot, J. Am. Ceram. Soc. **84**, 2997 (2001).